Hindawi
Material Design & Processing Communications
Volume 2022, Article ID 2623601, 8 pages
https://doi.org/10.1155/2022/2623601

Research Article

Variation of Poisson's Ratio with Axial Strain for Three-Dimensional Reentrant Auxetic Structures

Dan Andrei Şerban

Department of Mechanics and Strength of Materials, Politehnica University of Timişoara, Romania

Correspondence should be addressed to Dan Andrei Şerban; dan.serban@upt.ro

Received 25 September 2021; Accepted 5 January 2022; Published 31 January 2022

Academic Editor: Guian Qian

This study presents numerical investigations of the influence of structural parameters on the variation of the Poisson ratio with axial strain for auxetic structures. Three-dimensional reentrant structures were considered with variable strut thickness to length ratio and reentrance angles. The variation of the volume, relative density, and relative stiffness with axial strain was also studied.

1. Introduction

Mechanical metamaterials consist of designed structures that have no natural counterpart, that exhibit superior mechanical properties with respect to conventional materials [1, 2]. The scope of the engineered cells and patterns is to overcome the issue of mechanical property scaling with density that occurs for regular structures: $E_{\text{str}}/E_{\text{sol}} \propto (\rho_{\text{str}}/\rho_{\text{sol}})^n$ (where E_{str} and ρ_{str} are the structure stiffness and density, and E_{sol} and ρ_{sol} are the stiffness and density of the solid) [2]. Practical applications of mechanical metamaterial cellular plastics are scarce due to the high expenses associated with their manufacturing, usually consisting of rapid prototyping (RP) [3–5]. However, if proven to possess outstanding properties, this class of materials can be used in high-end applications, where the cost of production is not considered a priority.

Negative Poisson ratios (that determine an expansion in tension and contraction in compression) were experimentally observed in pyrites and single crystals in the beginning of the 20$^{\text{th}}$ century [6], and later in biological tissues [7] and composite laminates [8]. The first theoretical auxetic structures were proposed by Alexander Kolpakov [9] and Robert Almgren [10] while Roderic Lakes obtained the first polymer foams that exhibit such characteristics [11]. The term "auxetic," referring to materials and structures that possess negative Poisson ratios, was first introduced by Ken Evans in 1991 [12].

Over the years, auxetic structures were predicted, observed, and designed for various sizes, from nanomaterials (such as carbon allotropes [13, 14], liquid crystal polymers [15], or metals [16]) to microstructured foams [17–19] and macroscale lattices [20–22].

Considering their unique structural characteristics, in comparison with conventional materials, auxetic structures exhibit higher shear and fracture resistance as well as improved hardness and indentation resistance [23, 24] . Consequently, auxetic structures have a very wide range of potential application fields, such as aerospace industry (nose cones, wing panels) [25], automotive industry (bumpers, cushions) [26], biomedical applications (wound pressure pads, artificial blood vessels and skins) [27], military applications (helmets, bullet-proof vests) [23], textile industry (functional fabrics, color-change straps) [28], or sports industry (footwear applications, protective equipment) [29].

A negative Poisson ratio for a structure can be achieved through a variety of shapes. There are several categories in which auxetic structures can be classified: reentrant structures, rolling-up structures [23], and star/triangle-shaped structures [30] represent some of the basic 2D auxetic geometries. Out of the abovementioned structures, reentrant

geometries can be patterned into 3D geometries with the least of effort [31].

2. The 3D Reentrant Structure

The structures analyzed in this work consisted of tessellated regular auxetic cells (struts of equal length) with square cross-section walls and three parameters: the reentrance angle α, the strut thickness $2t$, and the strut length l (Figure 1). Considering that the theoretical structures have no defects, size effect is nonexistent; thus, the two variable parameters of the designed structures are the reentrance angle α and the strut thickness to strut length ratio t/l.

For this study, the reentrance angle α was varied between 65° (the lowest angle value that allowed clearance between the vertical struts) and 75° while the t/l ratio was varied between 0.3 and 0.7.

2.1. Relative Density. The relative density of the structures $\tilde{\rho}/\rho_s$ is expressed as the ratio between the density of the structure and the density of the solid. This relation can be extrapolated for any base material through expressing the relative density as the ratio between the volume of the structure $V_{\text{structure}}$ and the volume of the circumscribed prism V_{prism} [3].

$$\frac{\tilde{\rho}}{\rho_s} = \frac{V_{\text{structure}}}{V_{\text{prism}}}[-]. \tag{1}$$

The variation of the relative density with the re-entrance angle α and the t/l ratio is depicted in Figure 2 while Equation (2) presents the surface equation that was fitted for the obtained data ($R^2 = 0.9997$).

$$\rho_{rel}\left(\alpha, \frac{t}{l}\right) = e^{\left(\frac{184.53}{\alpha}+1.84\ \ln\ \left(\frac{t}{l}\right)-4.405\right)}. \tag{2}$$

3. Results

Numerical analyses were performed on the designed structures that were generated using the parameter variation presented in Table 1. A total of 50 analyses were performed (25 for tensile loadings and 25 for compressive loadings).

For the material model, a isotropic linear elastic formulation was used with Young's modulus $E_{\text{solid}} = 1500$ MPa and a Poisson's ratio $\nu_{\text{solid}} = 0.3$, corresponding an ABS compound (VeroWhitePlus RGD835) used in photopolymerization rapid prototyping [3]. The analyses were performed in Abaqus using the *Standard* solver. The models were meshed with second order tetrahedral elements (C3D10) with varying sizes to ensure a number of at least 4 elements per cross section.

During the analyses, the displacements variation with step time of the most outer nodes of the structure was recorded (d_1 and d_2, respectively) for all three directions, the length of the sides of the circumscribed prism $(x(t), y(t), z(t))$ resulting from the subtraction of the two values

$$x(t) = d_1^x(t) - d_2^x(t)\ y(t) = d_1^y(t) - d_2^y(t)\ z(t) = d_1^z(t) - d_2^z(t). \tag{3}$$

Subsequently, the nominal strains along the three directions were calculated with the relations:

$$\varepsilon_x(t) = \frac{x(t) - x_0}{x_0}\ \varepsilon_y(t) = \frac{y(t) - y_0}{y_0}\ \varepsilon_z(t) = \frac{z(t) - z_0}{z_0}. \tag{4}$$

Poisson's ratios with respect to the xOy pane (ν_{xy}) and the zOy plane (ν_{zy}) were observed to be equal and are expressed with the relation

$$\nu_{xy}(t) = \nu_{zy}(t) = \nu(t) = -\frac{\varepsilon_x(t)}{\varepsilon_y(t)} = -\frac{\varepsilon_z(t)}{\varepsilon_y(t)}. \tag{5}$$

3.1. Size Effect. In order to reduce computational time, a study was performed in order to determine the smallest structure that produces accurate results. For this purpose, structures varying from one cell up to $8 \times 8 \times 7$ cells were investigated (Figure 3).

The results of Poisson's ratio variation with strain (Figure 4) show a slight difference between the structure sizes, more noticeable in compression. Considering the relative errors and simulation times, it was decided that for the rest of the study, a $3 \times 3 \times 7$ structure will be used.

3.2. Poisson's Ratio Variation with Structural Parameters. The variation of Poisson's ratio with strain is due to the modification of the reentrance angle α with the axial strain $\varepsilon_y(t)$. For compressive loadings, Poisson's ratio increases with the increase in strain (the reentrance angle diminishing) while for tensile loadings, Poisson's ratio decreases with the increase in strain (due to the augmentation of the reentrance angle). When the reentrance angle reaches values larger than 90°, Poisson's ratio becomes positive, and the structures ceases to be auxetic. A typical variation of Poisson's ratio with axial strain for various values of the reentrance angle is presented in Figure 5 for a t/l ratio of 0.5.

For design purposes, the variation of Poisson's ratio with the initial reentrance angle and with strain can be expressed as a surface for each t/l ratio. The surfaces were fitted for Equation (6) with the coefficients being presented in Table 2.

$$\nu(\alpha, \varepsilon_y) = a + b\alpha + c\varepsilon_y + d\alpha^2 + f\varepsilon_y^2 + g\alpha\varepsilon_y. \tag{6}$$

A graphical depiction of the resulted surfaces is presented in Figure 6.

3.3. Volume and Relative Density Change. The variation of the volume of a structure with strain can be defines as

$$V(\varepsilon_x, \varepsilon_y, \varepsilon_z) = x_0(1 + \varepsilon_x(t)) \bullet y_0(1 + \varepsilon_y(t)) \bullet z_0(1 + \varepsilon_z(t)). \tag{7}$$

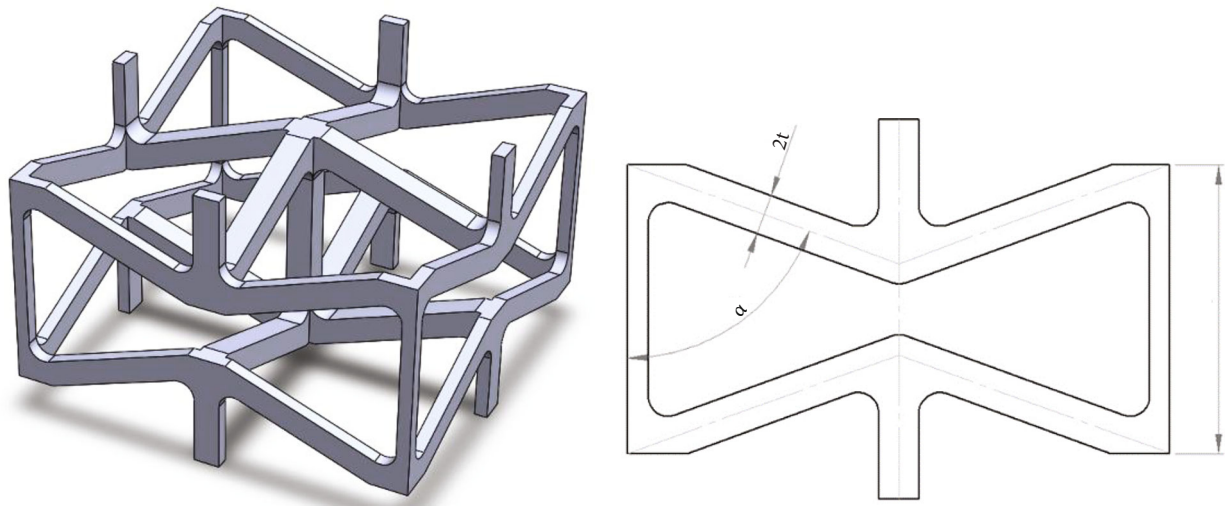

(a) (b)

Figure 1: Auxetic cell (a) and structural parameters (b).

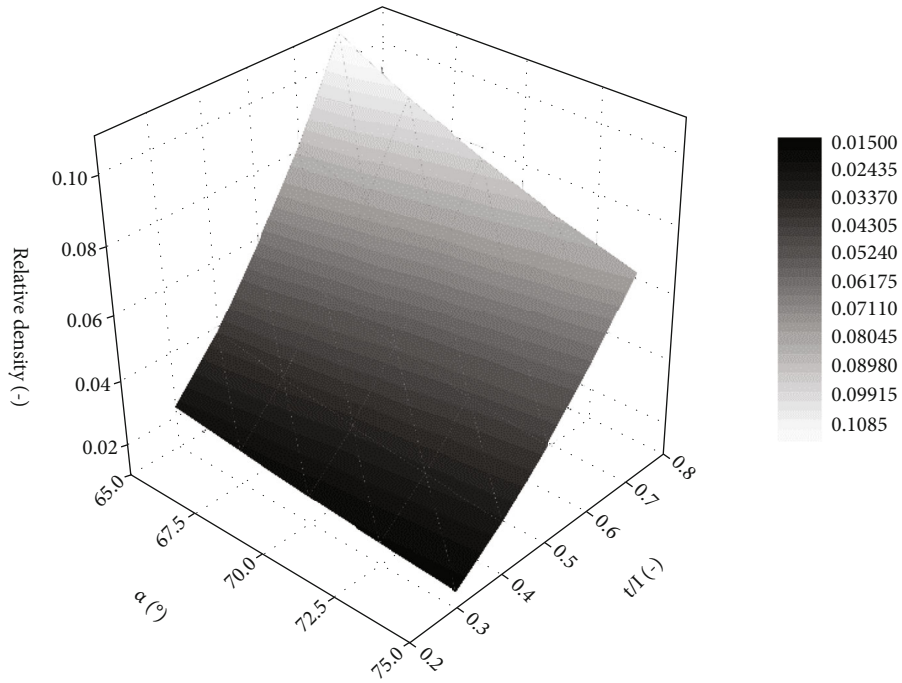

Figure 2: Variation of relative density with the reentrance angle α and the t/l ratio.

Considering the initial circumscribed volume of the structure $V_0 = x_0 \bullet y_0 \bullet z_0$, the relative volume of the structure at a given strain can be expressed as

$$V_{rel}(\varepsilon_x, \varepsilon_y, \varepsilon_z, t) = \frac{V(\varepsilon_x, \varepsilon_y, \varepsilon_z)}{V_0} = (1 + \varepsilon_x(t)) \bullet (1 + \varepsilon_y(t)) \bullet (1 + \varepsilon_z(t)). \quad (8)$$

Table 1: Auxetic structure parameters.

α [°]	t/l [–]
65	0.3
67.5	0.4
70	0.5
72.5	0.6
75	0.7

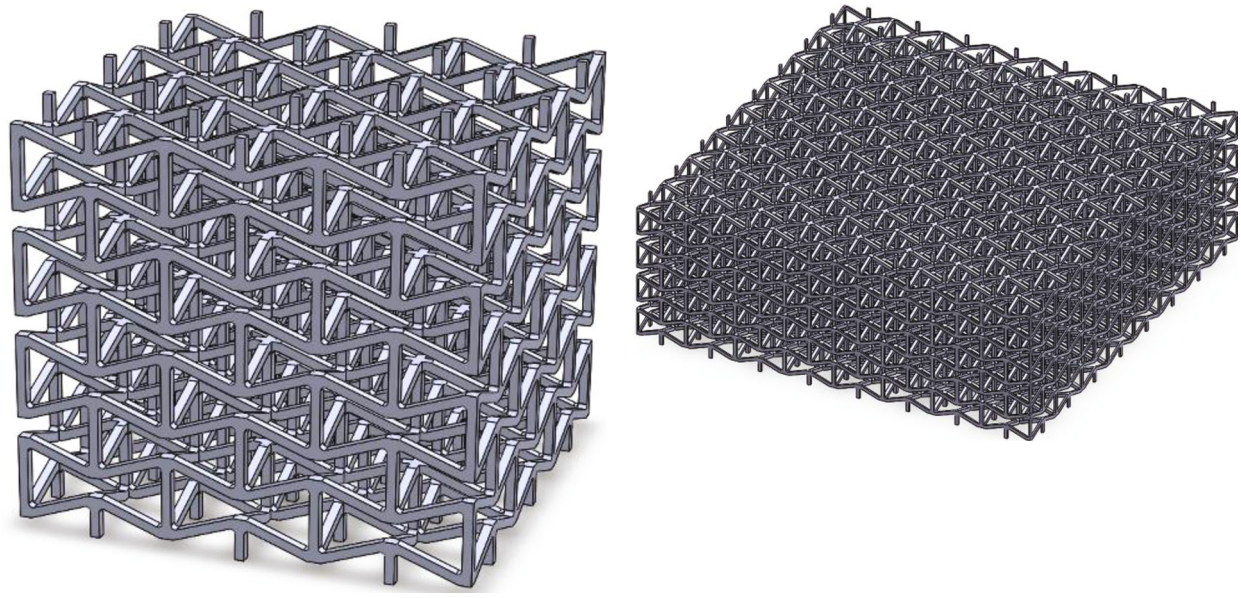

(a) (b)

Figure 3: Auxetic structures of $3 \times 3 \times 7$ cells (a) and $8 \times 8 \times 7$ (b).

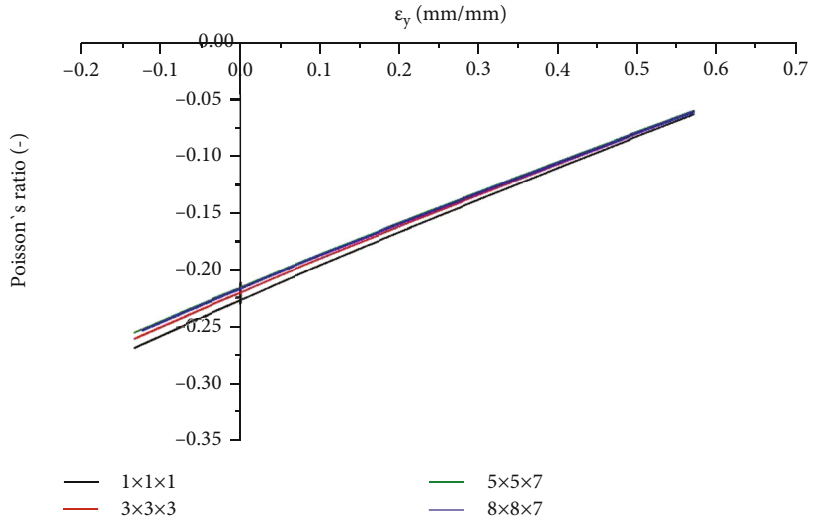

Figure 4: Variation of Poisson's ratio with axial strain for various structure sizes.

Considering Equation (5), the strains along the x and z directions will become

$$\varepsilon_x = \varepsilon_z = -\nu(\varepsilon_y) \bullet \varepsilon_y. \tag{9}$$

Introducing Equation (9) in Equation (8) yields

$$V_{\text{rel}}(\varepsilon_y) = \left(1 - \nu(\varepsilon_y) \bullet \varepsilon_y\right)^2 \bullet (1 + \varepsilon_y). \tag{10}$$

An example for the variation of the relative volume of the circumscribed prism with axial strain is presented in Figure 7(a)) for a t/l ratio of 0.7.

Considering the definition of the relative density (Equation (1)) and the variation of the circumscribed volume with strain (Equation (7)), the former's variation with strain is presented in Equation (11).

$$\rho_{rel}(\varepsilon_x, \varepsilon_y, \varepsilon_z) = \frac{V_{str}}{x_0(1 + \varepsilon_x) \bullet y_0(1 + \varepsilon_y) \bullet z_0(1 + \varepsilon_z)}. \tag{11}$$

Figure 7(b) depicts the variation of the relative density with strain for a t/l ratio of 0.7 showing an exponential increase in compression and decrease in tension.

3.4. Relative Stiffness. In order to evaluate the stiffness of the structures, the true stress and logarithmic strain must be

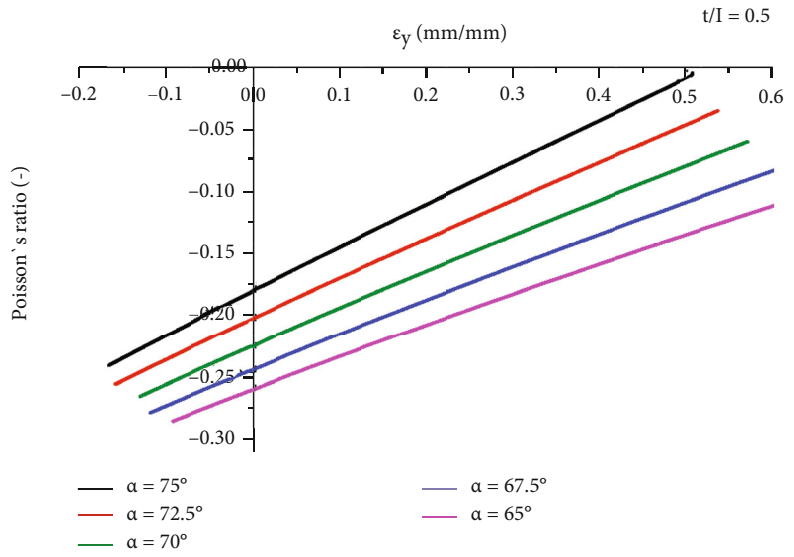

Figure 5: Variation of Poisson's ratio with the reentrance angle and axial strain for $t/l = 0.5$.

Table 2: Surface equation coefficients.

t/l	a	b	c	d	f	g
0.3	0.1935	−0.0211	−0.2906	0.0002	−0.0422	0.0091
0.4	0.4715	−0.0284	−0.3064	0.0003	−0.0366	0.009
0.5	0.3231	−0.0238	−0.3195	0.0002	−0.0323	0.009
0.6	0.4775	−0.0275	−0.3562	0.0002	−0.0275	0.0092
0.7	0.6844	−0.0326	−0.3937	0.0003	−0.0242	0.0095

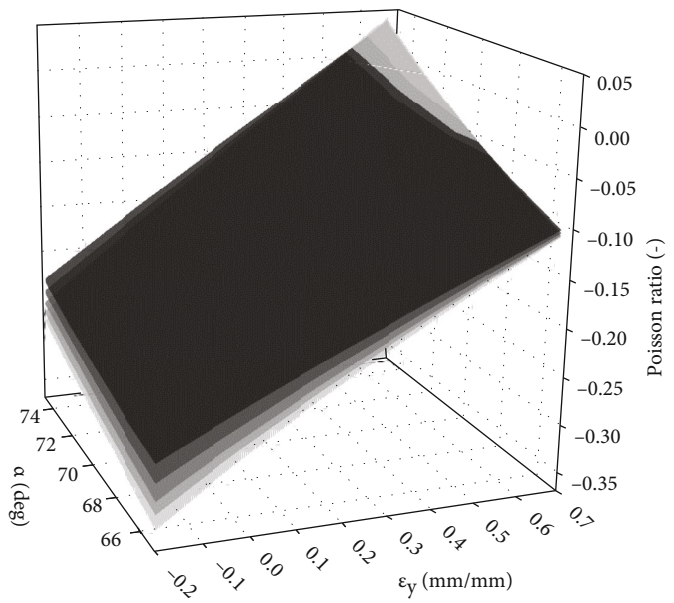

Figure 6: Variation of Poisson's ratio with the reentrance angle and axial strain for various t/l ratios.

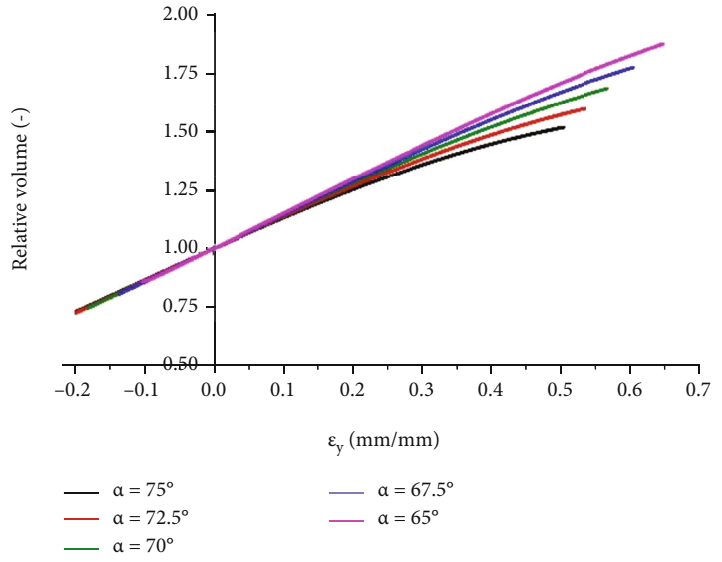

(a)

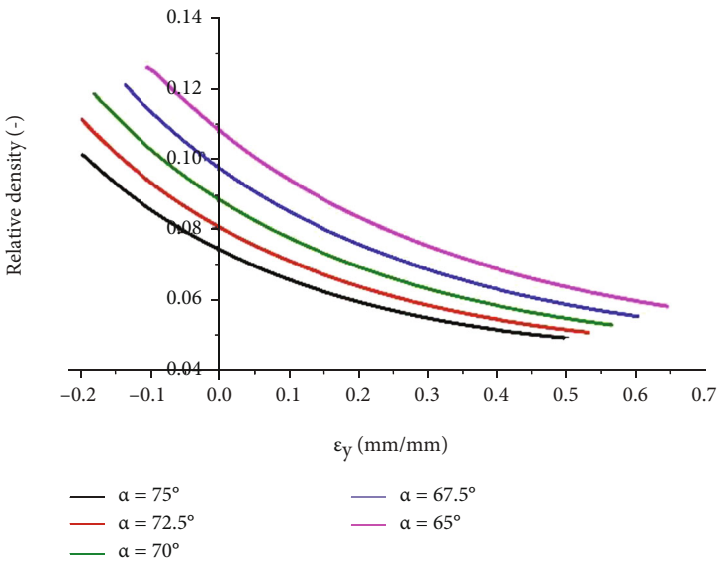

(b)

Figure 7: Relative volume of the circumscribed prism (a) and relative density (b) variation with strain for $t/l = 0.7$.

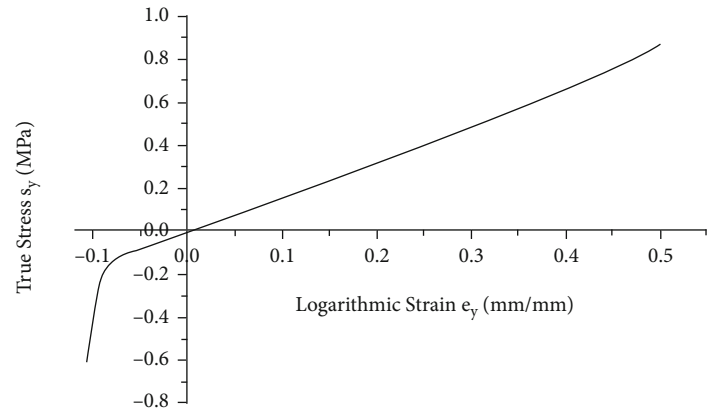

Figure 8: True stress variation with logarithmic strain for the structure with $\alpha = 65°$ and $t/l = 0.7$.

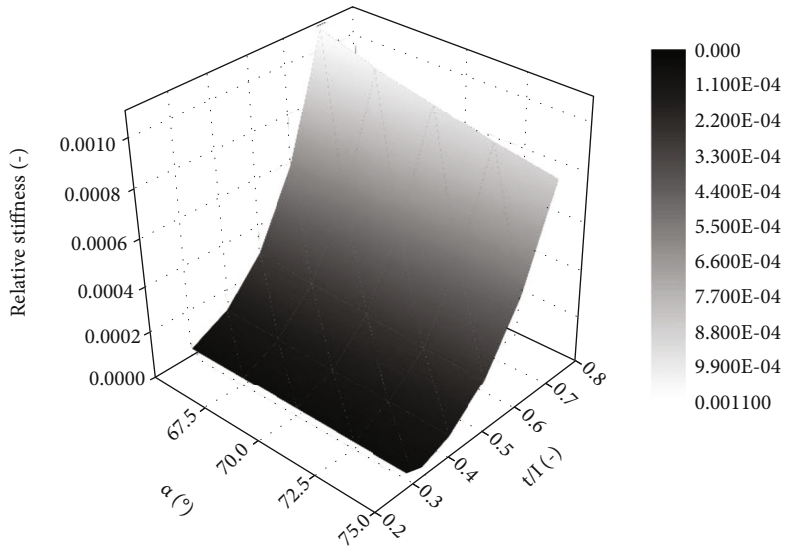

Figure 9: Variation of the relative stiffness with the re-entrance angle and t/l ratio.

determined. The true stress s_y is expressed as the recorded force in the fixed nodes F divided by the instantaneous area:

$$s_y(t) = \frac{F(t)}{x_0(1+\varepsilon_x(t))\bullet z_0(1+\varepsilon_z(t))}. \tag{12}$$

The logarithmic (Hencky) strain e_y is expressed as

$$e_y(t) = \ln\left(\varepsilon_y + 1\right). \tag{13}$$

An example of a true stress-logarithmic strain curve is presented in Figure 8 for the structure with $\alpha = 65°$ and $t/l = 0.7$. A nonlinear response is observed due to the volume change. In addition, for strain below0.08 mm/mm, a sudden increase in the absolute stress values is recorded, due to the contact between the struts of the structure.

The stiffness of the structure $\tilde{E}$ corresponds to the slope of the stress-strain curve and is evaluated as the variation of the true stress divided by the variation of the corresponding logarithmic strain (for small strain values).

$$\tilde{E} = \frac{\mathrm{d}s_y}{\mathrm{d}e_y} = \frac{s_y(t_1) - s_y(t_0)}{e_y(t_1) - e_y(t_0)}. \tag{14}$$

The relative stiffness of the structure is expressed as the stiffness of the structure divided by the stiffness of the solid.

$$E_{\mathrm{rel}} = \frac{\tilde{E}}{E_s}. \tag{15}$$

The variation of the relative stiffness of the structures with the reentrance angle and the t/l ratio is presented in Figure 9.

The surface depicted in Figure 9 was fitted for the Equation (16) with $R^2 = 0.9992$:

$$E_{rel}\left(\alpha, \frac{t}{l}\right) = \mathrm{e}^{\left(\frac{109.66}{\alpha} + 3.95\ \ln\left(\frac{t}{l}\right) - 7.109\right)}. \tag{16}$$

4. Discussions and Conclusions

This work presents the influence of the structural parameters (reentrence angle α and the thickness to lenght ratio t/l) on the stiffness, Poisson's ratio and density of auxetic structures. Due to the change in values of the reentrance angle value during deformation, a variation of the Poisson's ratio and of the relative density with strain is observed. Considering the increase in both values with the increase in compressive strain, this class of materials is expected to perform better than conventional cellular structures in energy absorption applications, as the material becomes denser and stronger as it is compressed.

Equations describing the variation of relative density and stiffness with the structural parameters are presented, which can be useful in the design stage of auxetic structures for specific applications. Future work will focus on the investigation of the influence of structural parameters on the energy absorption of the investigated structures, incorporating more advanced constitutive models, which account for damage and failure.

Data Availability

The data supporting the results can be provided at request.

Conflicts of Interest

The author declares that there is no actual or potential conflict of interest in relation to this article.

Acknowledgments

This study was funded through the framework of the grant from the Romanian National Authority for Scientific Research, CNCS–UEFISCDI, project code PN-III-P1-1.1-PD-2016-0445, Grant number 13/2018.

References

[1] X. Yu, J. Zhou, H. Liang, Z. Jiang, and L. Wu, "Mechanical metamaterials associated with stiffness, rigidity and compressibility: a brief review," *Progress in Materials Science*, vol. 94, pp. 114–173, 2018.

[2] X. Zheng, H. Lee, T. Weisgraber et al., "Ultralight, ultrastiff mechanical metamaterials," *Science*, vol. 344, no. 6190, pp. 1373–1377, 2014.

[3] D. A. Şerban, R. Negru, S. Sărăndan, G. Belgiu, and L. Marşavina, "Numerical and experimental investigations on the mechanical properties of cellular structures with open Kelvin cells," *Mechanics of Advanced Materials and Structures*, vol. 28, no. 13, pp. 1367–1376, 2021.

[4] L. Collini, C. Ursini, and A. Kumar, "Design and optimization of 3D fast printed cellular structures," *Material Design & Processing Communications*, vol. 3, no. 4, article e227, 2021.

[5] W. Radlof, C. Benz, and M. Sander, "Numerical and experimental investigations of additively manufactured lattice structures under quasi-static compression loading," *Material Design & Processing Communications*, vol. 3, no. 3, article e164, 2021.

[6] T.-C. Lim, *Auxetic Materials and Structures*, Springer Science +Business Media, Singapore, 2015.

[7] D. Veronda and R. Westmann, "Mechanical characterization of skin-finite deformations," *Journal of Biomechanics*, vol. 3, no. 1, pp. 111–124, 1970.

[8] S. Tsai and H. Han, *Introduction to Composite Materials*, Lancaster, Technomic, 1980.

[9] A. Kolpakov, "Determination of the average characteristics of elastic frameworks," *Journal of Applied Mathematics and Mechanics*, vol. 49, no. 6, pp. 739–745, 1985.

[10] R. Almgren, "An isotropic three-dimensional structure with Poisson's ratio =−1," *Journal of Elasticity*, vol. 15, pp. 427–430, 1985.

[11] R. Lakes, "Foam structures with a negative Poisson's ratio," *Science*, vol. 235, no. 4792, pp. 1038–1040, 1987.

[12] K. Evans, "Auxetic polymers: a new range of materials," *Endeavour*, vol. 15, no. 4, pp. 170–174, 1991.

[13] W. Wang, C. He, L. Xie, and Q. Peng, "The temperature-sensitive anisotropic negative Poisson's ratio of carbon honeycomb," *Nanomaterials*, vol. 9, no. 4, p. 487, 2019.

[14] M. Li, Y. Liu, and R. Li, "Design and prediction of a novel two-dimensional carbon nanostructure with in-plane negative Poisson's ratio," *Journal of Nanomaterials*, vol. 2019, Article ID 8618159, 2019.

[15] K. Evans, M. Nkansah, I. Hutchinson, and S. Rogers, "Molecular network design," *Nature*, vol. 353, p. 124, 1991.

[16] V. A. Gorodtsov and D. S. Lisovenko, "Auxetics among materials with cubic anisotropy," *Mechanics of Solids*, vol. 55, no. 4, pp. 461–474, 2020.

[17] J. N. Grima, R. Gatt, N. Ravirala, A. Alderson, and K. E. Evans, "Negative Poisson's ratios in cellular foam materials," *Materials Science and Engineering A*, vol. 426, pp. 214–218, 2006.

[18] Y. Li and C. Zeng, "On the successful fabrication of auxetic polyurethane foams: materials requirement, processing strategy and conversion mechanism," *Polymer*, vol. 87, pp. 98–107, 2006.

[19] R. Brighenti, "Smart behaviour of layered plates through the use of auxetic materials," *Thin-Walled Structures*, vol. 84, pp. 432–442, 2014.

[20] M. Grujicic, R. Galgalikar, J. Snipes, R. Yavari, and S. Ramaswami, "Multi-physics modeling of the fabrication and dynamic performance of all-metal auxetic-hexagonal sandwich-structures," *Materials and Design*, vol. 51, pp. 113–130, 2013.

[21] A. Spagnioli, R. Brighenti, M. Lanfranchi, and F. Soncini, "On the auxetic behaviour of metamaterials with re-entrant cell structurs," *Procedia Engineering*, vol. 109, pp. 410–417, 2015.

[22] A. Indreş, D. Constantinescu, and O. Mocian, "Bending behavior of 3D printed sandwich beams with different core topologies," *Material Design & Processing Communications*, vol. 3, no. 4, article e252, 2021.

[23] M. Assidi and J. Ganghoffer, "Composites with auxetic inclusions showing both an auxetic behavior and enhancement of their mechanical properties," *Composite Structures*, vol. 94, no. 8, pp. 2373–2382, 2012.

[24] S. Mohsenizadeh, R. Alipour, M. F. N. A. Shokri Rad, and Z. Ahmad, "Crashworthiness assessment of auxetic foam-filled tube under quasi-static axial loading," *Materials and Design*, vol. 88, pp. 258–268, 2015.

[25] Z. Wang, A. Zulifqar, and H. Hu, "Auxetic composites in aerospace engineering," in *Advanced Composite Materials for Aerospace Engineering*, pp. 213–240, Woodhead Publishing, 2016.

[26] W. Liu, N. Wang, T. Luo, and Z. Lin, "In-plane dynamic crushing of re-entrant auxetic cellular structure," *Materials and Design*, vol. 100, pp. 84–91, 2016.

[27] M. Ali, J. Busfield, and I. Rehman, "Auxetic oesophageal stents: structure and mechanical properties," *Journal of Materials Science: Materials in Medicine*, vol. 25, no. 2, pp. 527–553, 2014.

[28] J. Smardzewski, R. Kłos, and B. Fabisiak, "Design of small auxetic springs for furniture," *Materials and Design*, vol. 51, pp. 723–728, 2013.

[29] M. Sanami, N. Raviral, K. Alderson, and A. Alderson, "Auxetic materials for sports applications," *Procedia Engineering*, vol. 72, pp. 453–458, 2014.

[30] J. Grima, R. Gatt, B. Ellul, and E. Chetcuti, "Auxetic behaviour in non-crystalline materials having star or triangular shaped perforations," *Journal of Non-Crystalline Solids*, vol. 356, no. 37-40, pp. 1980–1987, 2010.

[31] L. Yang, O. Harrysson, H. West, and D. Cormier, "Mechanical properties of 3D re-entrant honeycomb auxetic structures realized via additive manufacturing," *International Journal of Solids and Structures*, vol. 69-70, pp. 475–490, 2015.